J Ther Eng, Vol. 9, No. 3, pp. 565−579, May, 2023

Journal of Thermal Engineering
Web page info: https://jten.yildiz.edu.tr
DOI: 10.18186/thermal.1293026

Journal of Thermal Engineering

Research Article

Performance comparison of basic and parallel double evaporator Organic Rankine Cycle integrated with solar based supercritical CO_2 cycle

Yunis KHAN[1,*], Radhey SHYAM MISHRA[1]

[1]*Department of Mechanical Engineering Delhi Technological University, Bawana Road New Delhi, 110042, India*

ARTICLE INFO

Article history
Received: 08 March 2021
Accepted: 09 June 2021

Keywords:
Performance comparison; ORC; PDORC; Solar Power Tower; Intercooled Cascade sCo_2 Cycle

ABSTRACT

Performance comparison of basic organic Rankine cycle (ORC) and parallel double evaporator ORC (PDORC) integrated with solar power tower (SPT) driven intercooled cascade sCO_2 (supercritical carbon dioxide) cycle was carried out in present study. The intercooled cascade sCO_2 cycle/ORC (configuration-1) and the intercooled cascade sCO_2 cycle/PDORC (configuration-2) were considered for comparison on basis of parametric analysis. The effects of SPT design parameters such as solar irradiation, solar receiver emittance, and concentration ratio on system performance were investigated. It was concluded that the addition of basic ORC and PDORC to the intercooled cascade sCO_2 cycle improved the thermal efficiency by 2.26% and 6.66% respectively at solar irradiation of 950 W/m^2. In the case of basic ORC and PDORC, the waste heat recovery ratios were 0.1197 and 0.1775, respectively. It was also discovered that configuration-2 performed better than configuration-1 in terms of waste heat recovery. The combined cycle's performance can be improved even more by lowering solar emittance and increasing the concentration ratio.

Cite this article as: Khan Y, Shyam Mishra R. Performance comparison of basic and parallel double evaporator Organic Rankine Cycle integrated with solar based supercritical CO_2 cycle. J Ther Eng 2023;9(3):565−579.

INTRODUCTION

Energy consumption used for the cooling and power generation increased drastically in recent years [1]. Consequently, fossil fuel consumption is continuously raising that leads to increase carbon emissions. However, fossil-fuel stocks are steadily decreasing. This leads to the challenge of finding clean and reliable energy resources [2]. There are currently numerous renewable energy resources being used to generate clean and ecofriendly power such as, solar, wind, biomass, and geothermal energy. Because of its availability, low cost and noise free operation, solar energy is more suitable in power generation among these renewable energy resources [3].

Solar collectors are used to collect sunlight for cooling, heating, and power generation [4].Concentrated solar collectors like parabolic trough collectors, dish collectors, heliostats, etc. are used for high temperature applications. Kalogirou [5] recorded parabolic trough collector (60−500°C), dish collector (750−1000°C), and

*Corresponding author.
*E-mail address: yuniskhan21@gmail.com

This paper was recommended for publication in revised form by Regional Editor Ahmet Selim Dalkılıç

heliostat (150–1500°C) working temperature range. Among other solar technologies, concentrated solar power (CSP) technology plays a key role in solving the current and future question of power generation in tropical countries through the use of solar heat that is readily accessible in nature [6].

The SPT is the latest technology amongst the various CSP technologies. SPT system consists of number of complex sub-systems such as receiver, 75-150 m high tower, thermal storage system (optional), heliostat field with per heliostat area of 50-150 m^2 and power conversion system. Solar radiation is centered on receiver by heliostat field where it is used to produce high temperature heat for power generation through a high energy cycle or for industrial process supply [7]. Several studies were performed on the SPT driven cycles such as combined recompression sCO_2 cycle and transcritical CO_2 (carbon dioxide) cycle [8], sCO_2 Brayton cycle [9], recompression sCO_2 with and without main compressor intercooling [10], triple combined cycle [11], multi generation combine cycle [12].

The CO_2 above its critical values (7.38 MPa, 30.9°C) is said to be sCO_2. Further, sCO_2 cycle is the cycle that can utilize the heat from various heat sources such as solar thermal energy, geothermal, coal power and natural gas [13]. A few researcher published articles on the basis of sCO_2 such as Khan and Mishra [14] conducted a study on the solar parabolic trough collector integrated combined partial heating sCO_2 cycle and ORC. They also investigated the effect of solar system on performance of the combined system. They came to the conclusion that adding ORC to the partial heating cycle increased thermal efficiency by 4.47%. The exergy efficiency of the combined system increased with the solar irradiation. Finally they also observed that R1233zd(E) is the best performing fluid among the other working fluids considered such as R1224 yd(Z), R1234ze(Z), R1234yf, R1234ze(E), and R1243zf. Also Khan and Mishra [15] compared standalone pre-compression sCO_2 cycle with combined ORC integrated with the SPT. It was found that thermal efficiency and power output of the standalone pre-compression sCO_2 cycle were improved by 4.51% and 4.52% respectively by addition of ORC as bottoming cycle. They also concluded that R227ea recovered highest heat among the considered working fluids. Besarati and Goswami [16] performed a comparative analysis of the various configurations of the sCO_2 cycle such as recompression, simple recuperated, and partial cooling cycle. They first compared the systems standalone and used ORC as the bottom cycle thereafter to recover the waste heat from all three cycles and compared it again. They concluded that the combined cycle achieved more than 50% thermal efficiency as well as the recompression cycle being the best performing cycle among the cycles considered. Khan and Mishra [41] carried out exergoeconomic analysis of the SPT driven pre-compression sCO_2 cycle and ORC. They observed R1336mzz(z) gave highest thermal efficiency, exergy efficiency and power output at 950W/m^2 of solar irradiation. Also in another study Khan and Mishra [42] performed thermal analysis of SPT driven recompression sCO_2 cycle with main compression intercooling combined with bottoming ORC using low global warming potential fluids. They found that after the addition of the ORC thermal efficiency of the combined cycle improved by 7-8% with reference conditions. Kim et al [17] also performed a comparative analysis on 12 different sCO_2 cycle configurations such as simple recuperated cycle, recompression, single heated cascade cycle, partial heating, dual cascade cycle, pre-compression, single heated cascade cycle with intercooler, intercooled dual heated cascade cycle, dual expansion cycle, dual heated and flow split cycles for triple heating cycle and partial recuperation cycle as land filling gas turbine bottoming. They found that pre-compression and recompression cycle had high thermal efficiency than other considered cycles. They also suggested for future research on combination of two cycles. Yu et al. [18] considered four configurations of the sCO_2 cycles such as pre-compression, simple recuperated, recompression cycle, and split flow recompression cycle, for recovering the waste heat from the internal combustion engine. Further, thermal efficiency and waste heat recovery ratio of the four systems were determined. The maximum waste heat recovery ratio for pre-compression and sCO_2 cycle recovery was found to be reached at 5.8 MPa and 7.65 MPa respectively. Furthermore, split flow cycle was found as best performing cycle with highest recovery ratio was 24.75%. Neises and Turchi [19] examined the cost, design, and performance of the three sCO_2 cycle configurations, such as simple cycle, recompression cycle and partial cooling cycle, driven by the molten salt solar power tower. As a result, highest thermal efficiency was achieved in case of the recompression cycle followed by partial cooling and a simple cycle. Partial cooling was found to be more costly than other cycles due to the high demand for turbo machinery.

One extra compressor and one intercooler are used in the cascade cycle with an intercooler [20] than in the single heated cascade cycle. Turbine work and compressor work are improved by the intercooling process, resulting in high thermal cycle efficiency compared to the basic cascade cycle for the same heat input [20]. As a result, due to the greater impact of increased thermal efficiency of the cycle than the decreased amount of absorbed heat, this cycle has 0.09MWe higher net produced work. This cycle, however, has not only more components than the partial heating cycle, but also comparable net work generated with the partial heating cycle [17].

Apart from this, ORC is the useful technology for the recovery of low temperature waste heat. ORC is used as a bottoming cycle in the current scenario. There are a few studies to support this comment such as Shaaban [21] carried out a solar integrated combined cycle study in which ORC and steam Rankine cycle were used as a bottoming

cycle for the recovery of waste heat. The author considered 15 working fluids in the ORC and found that R1234ze(Z) was the best fluid in terms of thermo-economic, environmental and safety considerations. Hoang [22] reviewed for application of the ORC as bottoming cycle to the exhaust waste heat recovery from diesel engines. They found that ORC can achieve up to 25% thermal efficiency, while combined system with diesel engine achieved up to 90% thermal efficiency. Song et al. [23] conducted a performance and optimization analysis of the combined cycle of sCO_2 and ORC. The effects of topping cycle recuperative ratio, pressure ratio on the performance of the bottoming ORC were examined. They resulted in an improvement in the thermal efficiency of the existing sCO_2 cycle by adding the ORC system. ORC system recovered completely residual heat. Apart from basic ORC, PDORC also suitable for recovering more waste heat as compared to basic ORC. PDORC produced more work than the basic ORC [24].

From the literature survey, it was observed that performance of the intercooled cascade sCO_2 cycle can be enhanced further by incorporating a low temperature bottoming ORC. However, detailed thermodynamic analysis of SPT driven combined intercooled cascade sCO_2 cycle and ORC is not present in the literature. Also no PDORC system was used as bottoming cycle in literature as waste heat recovery cycle. Therefore, present study deals with thermodynamic analysis of the combined cycle driven by solar power tower. Further, the performance of the standalone intercooled cascade sCO_2 cycle was compared by incorporating the basic ORC (configuration-1) and PDORC (configuration-2) as bottoming cycle along with parametric analysis of the proposed combined cycles was also conducted and best configuration for waste heat recovery was found out. This demonstrates the novelty of the present research. A computer program in engineering equation solver software was made to simulate the system. Exergy, thermal efficiency, net output work were considered as performance parameters of the proposed systems. The effects of the system variable such as SPT design parameters (solar irradiation or direct normal irradiation (DNI), solar receiver emittance, concentration ratio), inlet temperature of the high temperature turbine, inlet temperature of compressors and inlet pressure of the compressor-1 on the system performance were investigated. At last waste heat recovery ratio for the both configurations was also investigated.

SYSTEM DESCRIPTION

Current study deals with two configurations for comparison. First configuration consist three subsystems such as solar system, intercooled cascade sCO_2 cycle [17] and bottoming basic ORC (configuration-1) as shown in Figure 1a. Another configuration also consist two subsystems same as first configuration but PDORC [24] as bottoming cycle (configuration-2) as shown in Figure 1b. Mixture of molten salt considered as the heat transfer fluid (HTF) in solar system. The sCO_2 stream is flowing in the intercooled cascade

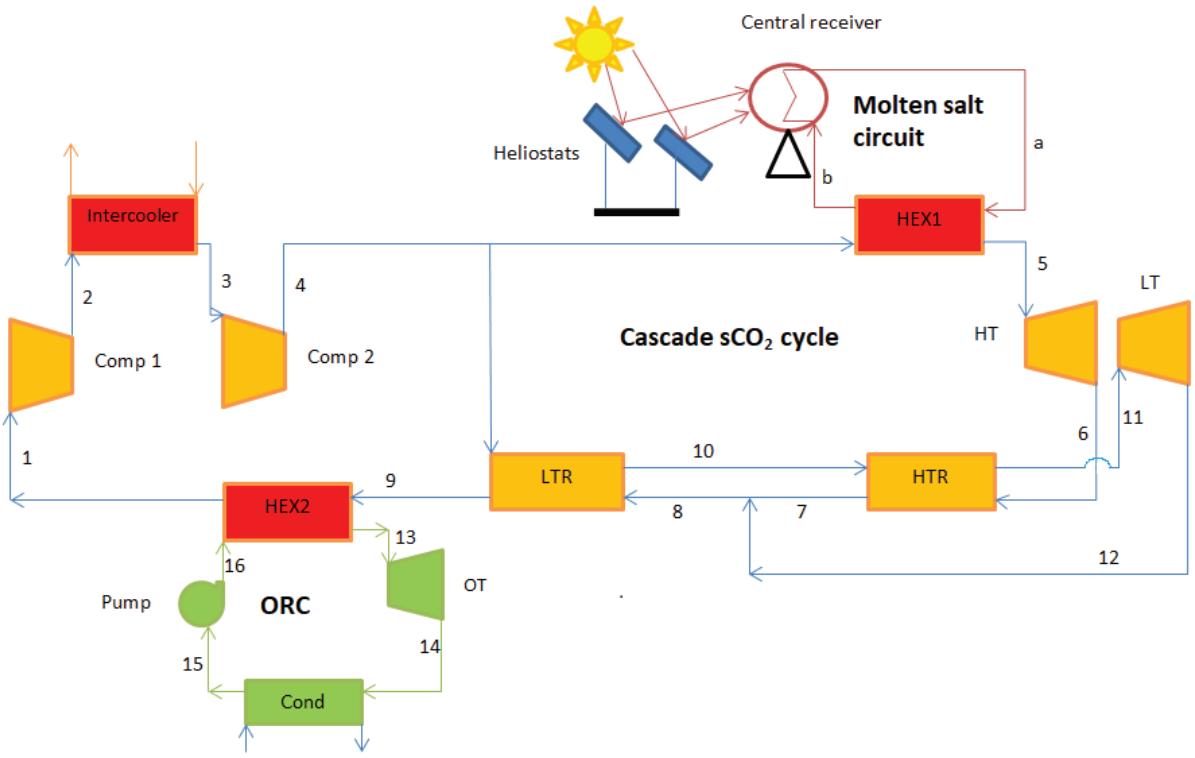

Figure 1a. Schematic diagram of SPT driven combined intercooled cascade $sCO_2$and ORC (configuration-1).

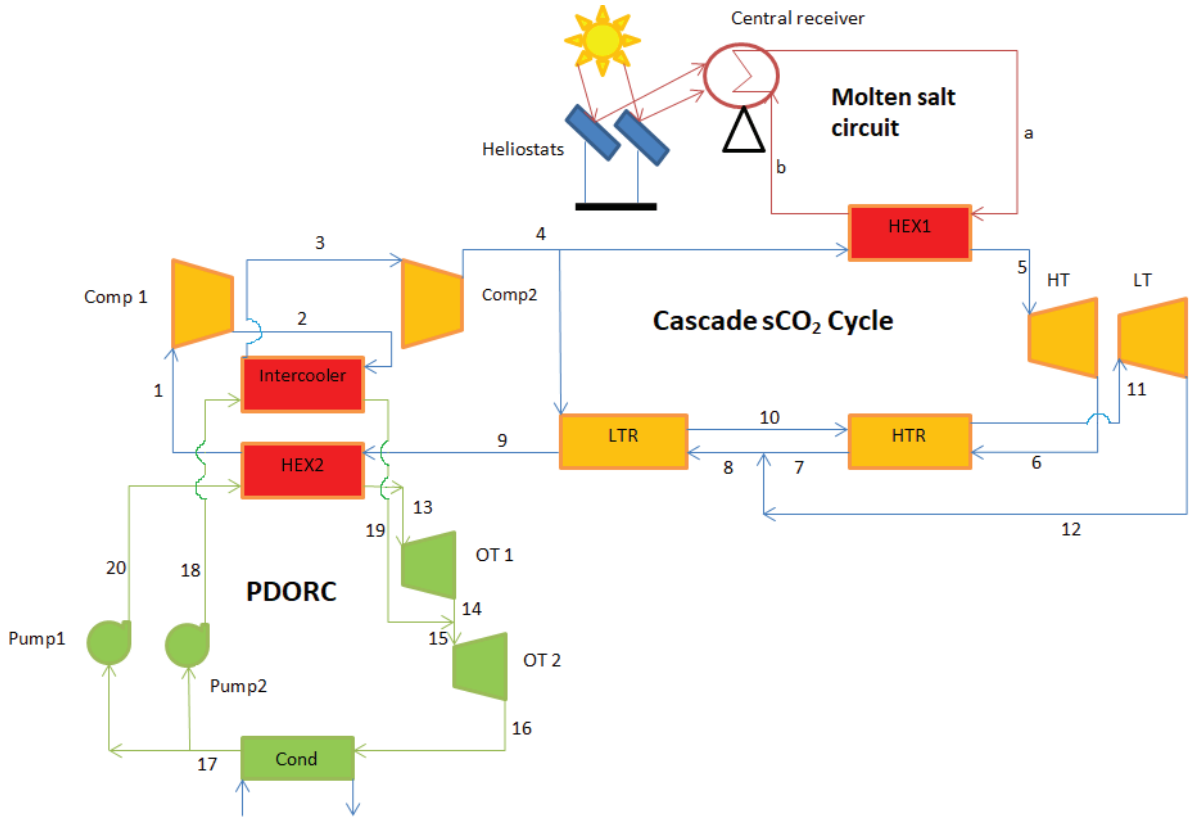

Figure 1b. Schematic diagram of SPT driven combined intercooled cascade sCO_2 with and PDORC (configuration-2)

cycle. After taking the heat through the heat exchanger-1 (HEX1) sCO_2 stream expanded in the high temperature turbine (HT). Expanded stream have much amount of heat therefore it is recuperated in the high temperature recuperator (HTR) then goes to the low temperature recuperator (LTR) after mixing with expanded stream coming from low temperature turbine (LT). After LTR some heat is still remain. This remaining heat is used by ORC through heat exchanger-2 (HEX2). Further, sCO_2 stream compressed through the compressor-1 (Comp 1) then perfectly intercooled, after this stream again compressed in compressor-2 (Comp 2). A fraction of total mass of sCO_2 stream goes to LTR and remaining goes to HEX1, this repeats again and again.

In the configuration-2 instead of basic ORC, the PDORC is used for recovering the waste heat from HEX2 and intercooler simultaneously as shown in Figure 1b. After getting the heat through HEX2 (It is possible to call it evaporator-1) organic working fluid (HFO1234yf) stream is expanded in organic turbine-1 (OT1), expanded stream mixes with the stream that is coming out from the intercooler (It is possible to call it evaporator-2). Total mass of R1234yf stream is expanded in the organic turbine-2 (OT2). After the condenser HFO1234yf stream splits in two parts, one part goes to the intercooler through the pump-2 to recover remaining part of the waste heat. Another part goes to the HEX2 for recovering the waste heat. Thus PDORC completed and repeated again and again. T-s diagrams of the intercooled cascade sCO_2 cycle, basic ORC and PDORC corresponding to the state points are shown in Figures 2a, 2b, and 2c respectively.

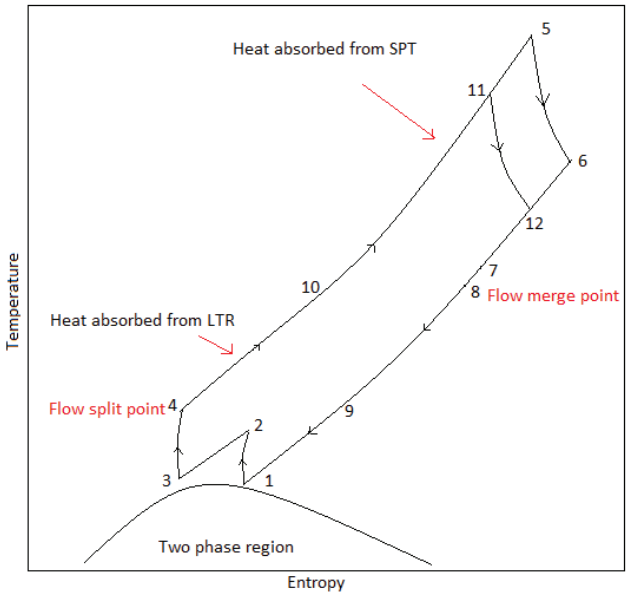

Figure 2a. T-s diagram of intercooled cascade sCO_2 cycle.

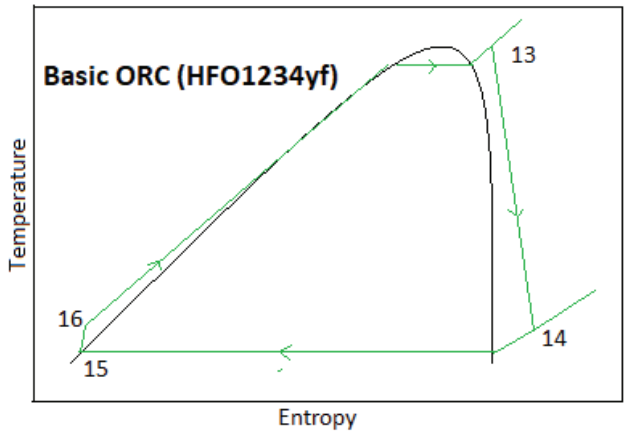

Figure 2b. T-s diagram of basic ORC using HFO1234yf fluid.

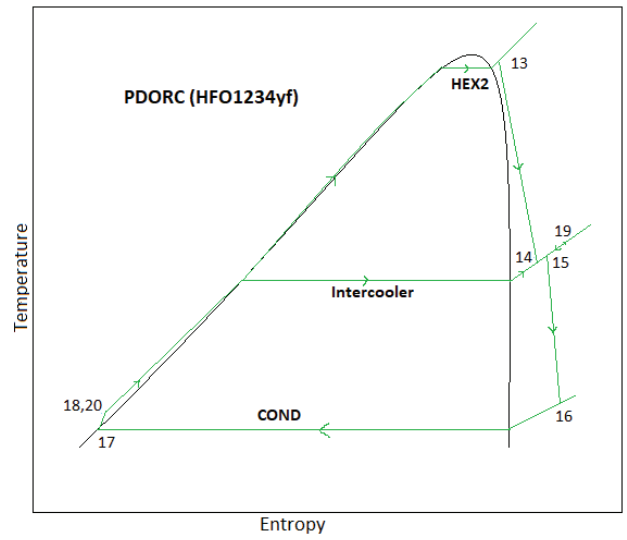

Figure 2c. T-s diagram of PDORC using HFO1234yf fluid.

Table 1. Input parameters for simulation of the proposed model

Geometric and operating parameters for SPT	
Direct normal irradiation	850 W/m^2 [14]
Sun temperature	4500 K [25]
Solar's multiple	2.8 [8]
Efficiency of heliostat	58.71 % [26]
Number of heliostat	141 [27]
Heliostat's total mirror area	9.04×7.89 [8]
Initial temperature difference	15 K [8]
Solar receiver's temperature approach	423.15 K [26]
Concentration ratio	900 [26]
Convective heat loss coefficient	10 W/m^2-K [26]
Tower height	74.62 m [27]
Convective heat loss factor	1 [26]
View factor	0.8 [26]
Absorptance	0.95 [26]
Thermal emittance	0.85 [26]
Input parameters for combined cycle	
HT inlet pressure	25 MPa [28]
HT inlet temperature	650 °C [8, 28]
Compressor-1 inlet pressure	7 –10.5 MPa [28, 29]
Compressor inlet temperature	32–38 °C [28, 29]
HT isentropic efficiency	0.88 [28, 29]
Compressor-1 isentropic efficiency	0.85 [28, 29]
Heat exchanger effectiveness	0.95 [16]
HTR and LTR effectiveness	0.95 [16]
sCO_2 topping cycle mass flow rate	1.6 kg/s
Mass flow rate in bottoming ORC	2.7 kg/s
ORC turbine inlet pressure	3 MPa [14, 15]
ORC turbine's Isentropic efficiency	0.8 [23]
ORC pump's Isentropic efficiency	0.7 [23]

THERMODYNAMIC ANALYSIS

Assumptions

Performance analysis of the SPT powered combined cycle was performed considering following assumptions to support the simulation;

(1) All system components are in a steady state conditions.
(2) Pressure and friction loss are neglected in each component and pipes.
(3) All thermodynamic processes are polytropic.
(4) Energy due to height and velocity of the each component is neglected
(5) Heliostat and receiver parameters are kept constant and assumed input data to support the simulation are listed in table 1.
(6) Molten salt temperature inlet to the HEX1 has been taken 700°C [29].
(7) Due to thermal losses, inlet temperature of HT is 50°C less than molten salt temperature inlets to the HEX1 [15]. (8) HFO1234yf has been selected as organic working fluid for the bottoming ORC and PDORC due to its ultra low GWP, ODP and high temperature stability [23].
(9) Mixture of molten salt is considered as HTF in SPT field which thermophysical properties are listed in table 2.

Table 2. Thermo-physical properties of molten salt ($MgCl_2$ - KCl) [30]

Parameters	Values
Density	1593 (kg/m^3)
Thermal conductivity	0.39 (W/m-K)
Specific heat capacity	1.028 (kJ/kg-K)
Solidification temperature	699 K

Thermal modeling of SPT

Thermal modeling equations of the proposed system were developed in this part based on the conservation of exergy and energy equations, taking into consideration of assumptions those are made in above section. Modeling equations for SPT have been taken from the previous studies [8,15]. Also each component has been treated as control volume.

Direct solar heat incidence upon heliostat field is defined as;

$$\dot{Q}_{solar} = DNI \cdot A_h \cdot N_h \quad (1)$$

Where, DNI is direct normal irradiation (DNI), A_h is single heliostat area (m^2) and N_h is the heliostats number. However, due to heliostat efficiency, some of that heat is lost in the surroundings. The amount of actual heat obtained through the heliostat field is therefore specified as;

$$\dot{Q}_h = \dot{Q}_{solar} \cdot \eta_h \quad (2)$$

Where, η_h is the efficiency of heliostat. This amount of heat is directed to the solar receiver where the heat transfer fluid flows. But in the atmosphere a part of the heat is lost. The heat available at the solar center receiver is therefore determined as;

$$\dot{Q}_r = \dot{Q}_h \cdot \eta_r = \dot{Q}_h - \dot{Q}_{loss,r} \quad (3)$$

Where, η_r is the receiver thermal efficiency, is defined as;

$$\eta_r = \alpha - \frac{\zeta \cdot f_{view} \cdot \sigma \cdot T_R^4 + h_{conv} \cdot f_{conv} \cdot (T_R - T_{air})}{DNI \cdot \eta_h \cdot CR} \quad (4)$$

Where, T_R is the solar receiver surface temperature and CR is concentrated ratio. ζ is the solar emittance. To calculate heat loss, this can be approximated as;

$$T_R = T_1 + \delta T_R \quad (5)$$

Where, T_1 is the turbine's inlet temperature and δT_R is approach temperature of solar receiver.

The operating and geometric parameters of the solar receiver and the heliostat field are listed in table 1.

Furthermore, exergy of the any system can be explained as maximum work obtainable from the system when system is brought to its dead conditions. Control volume exergy balance equation can be determined as [31];

$$\sum \left(1 - \frac{T_0}{T_j}\right) \dot{Q}_j - \dot{W}_{cv} - \sum(\dot{m}_i E_i) - \sum(\dot{m}_e E_e) - \dot{ED} = 0 \quad (6)$$

Where, $\dot{ED}$ is the exergy destruction rate and subscript j refers to thermal property at particular state. Solar exergy inlet to the combined system is determined as;

$$\dot{E}_{solar} = \left(\frac{\dot{Q}_r}{\eta_h \cdot \eta_r}\right) \cdot E_s \quad (7)$$

Where, E_s is the dimensionless maximum useful work obtained from the solar irradiation. E_s is expressed as;

$$E_s = 1 + \frac{1}{3}\left(\frac{T_0}{T_{su}}\right)^4 - \frac{4}{3}\left(\frac{T_0}{T_{su}}\right)(1 - \cos\beta)^{1/4} \quad (8)$$

Where, T_{su} and T_0 are the sun and reference temperature respectively. β is the sun's disc subtended half cone angle. Its value has been taken 0.005 rad on solar energy limiting efficiency [32]. Further, in the receiver, useful exergy obtained by the molten salt is defined as

$$\dot{E}_r = \dot{m}_{ms} \cdot Cp_{ms} \cdot \left[(T_b - T_a) - \left(T_0 \cdot \ln\frac{T_b}{T_a}\right)\right] \quad (9)$$

Further chemical exergy of the system is constant throughout. After neglecting energy due to velocity and height, specific physical exergy at jth point is defined as [8, 33];

$$E_j = (h_j - h_0) - T_0(h_j - s_0) \quad (10)$$

Thermal modeling of combined cycle

Based on the energy balance equations and control volume approach, equations for the each component of the cycles were developed and listed in table 3.

Net power output obtained from the combined cycle is defined as;

$$\dot{W}_{net\ standalone} = \dot{W}_{HT} + \dot{W}_{LT} - \dot{W}_{Comp\ 1} - \dot{W}_{Comp\ 2} \quad (11)$$

$$\dot{W}_{net\ conf\ 1} = \dot{W}_{HT} + \dot{W}_{LT} + \dot{W}_{OT} - \dot{W}_{Comp\ 1} - \dot{W}_{Comp\ 2} - \dot{W}_{pump} \quad (12)$$

$$\dot{W}_{net\ conf\ 2} = \dot{W}_{HT} + \dot{W}_{LT} + \dot{W}_{OT\ 1} + \dot{W}_{OT\ 2} - \dot{W}_{Comp\ 1} - \dot{W}_{Comp\ 2} - \dot{W}_{pump\ 1} - \dot{W}_{pump\ 2} \quad (13)$$

Solar powered combined cycle's thermal efficiency is determined as;

Table 3. Governing equations of each component of the cycles

Cascade sCO_2 cycle with intercooling	
Components	**Equations**
HEX1	$\dot{Q}_r = \dot{Q}_{HEX1} = \dot{m}_{ms} \cdot Cp_{ms} \cdot (h_b - h_a) = x \cdot \dot{m}_{SCO2} \cdot (h_5 - h_4)$
HT	$\dot{W}_{HT} = x \cdot \dot{m}_{SCO2} \cdot (h_5 - h_{6s}) \cdot \eta_{HT}$
LT	$\dot{W}_{LT} = (1 - x) \cdot \dot{m}_{SCO2} \cdot (h_{11} - h_{12s}) \cdot \eta_{LT}$
HTR	$\dot{Q}_{HTR} = x \cdot \dot{m}_{sCO2} \cdot (h_6 - h_7) = (1\text{-}x) \cdot \dot{m}_{sCO2} \cdot (h_{11} - h_{10})$
LTR	$\dot{Q}_{LTR} = \dot{m}_{sCO2} \cdot (h_8 - h_9) = (1\text{-}x) \cdot \dot{m}_{sCO2} \cdot (h_{10} - h_4)$
Comp 1	$\dot{W}_{Comp1} = \frac{\dot{m}_{sCO2} \cdot (h_{2s} - h_1)}{\eta_{comp1}}$
Comp 2	$\dot{W}_{Comp2} = \frac{\dot{m}_{sCO2} \cdot (h_{3s} - h_2)}{\eta_{comp2}}$
Basic ORC	
OT	$\dot{W}_{OT} = \dot{m}_{ORC} \cdot (h_{13} - h_{14s}) \cdot \eta_{OT}$
Cond	$\dot{Q}_{cond} = \dot{m}_{ORC} \cdot (h_{14} - h_{15})$
Pump	$\dot{W}_{pump} = \frac{\dot{m}_{ORC} \cdot (h_{16s} - h_{15})}{\eta_{pump}}$
HEX2	$\dot{Q}_{HEX2} = \dot{m}_{SCO2} \cdot (h_9 - h_1) = \dot{m}_{ORC} \cdot (h_{13} - h_{16})$
PDORC	
OT1	$\dot{W}_{OT1} = \dot{m}_{ORC} \cdot (h_{13} - h_{14s}) \cdot \eta_{OT}$
OT2	$\dot{W}_{OT2} = \dot{m}_{ORC} \cdot (h_{15} - h_{16s}) \cdot \eta_{OT}$
Cond	$\dot{Q}_{cond} = \dot{m}_{ORC} \cdot (h_{16} - h_{17})$
Pump1	$\dot{W}_{pump1} = \frac{\dot{m}_{ORC} \cdot (h_{20s} - h_{17})}{\eta_{pump}}$
Pump2	$\dot{W}_{pump2} = \frac{\dot{m}_{ORC} \cdot (h_{18s} - h_{17})}{\eta_{pump}}$
HEX2	$\dot{Q}_{HEX2} = \dot{m}_{SCO2} \cdot (h_9 - h_1) = \dot{m}_{ORC} \cdot (h_{13} - h_{20})$
Intercooler	$\dot{Q}_{Intercooler} = \dot{m}_{sCO2} \cdot (h_2 - h_3) = \dot{m}_{ORC} \cdot (h_{19} - h_{18})$

$$\eta_{th\ standalone} = \frac{\dot{W}_{net\ standalone}}{\dot{Q}_{solar}} \quad (14)$$

$$\eta_{th\ conf\ 1} = \frac{\dot{W}_{net\ conf1}}{\dot{Q}_{solar}} \quad (15)$$

$$\eta_{th\ conf\ 2} = \frac{\dot{W}_{net\ conf\ 2}}{\dot{Q}_{solar}} \quad (16)$$

Furthermore, in this section exergy analysis of the combined system also to be discussed. Exergy destruction in each component is determined by applying the exergy balance Eq. (6) for each component after assuming no heat loss in the component [31].

After calculating the exergy destruction rate for each component, total exergy destruction rate for the combined cycle is calculated as;

$$\dot{E}D_{standalone} = \dot{E}D_{HEX1} + \dot{E}D_{HT} + \dot{E}D_{LT} + \dot{E}D_{HTR} + \dot{E}D_{comp\ 2} + \dot{E}D_{comp\ 1} + \dot{E}D_{LTR} + \dot{E}D_{HEX2} + \dot{E}D_{intercooler} \quad (17)$$

$$\dot{E}D_{conf\ 1} = \dot{E}D_{HEX1} + \dot{E}D_{HT} + \dot{E}D_{LT} + \dot{E}D_{HTR} + \dot{E}D_{comp\ 2} + \dot{E}D_{comp\ 1} + \dot{E}D_{LTR} + \dot{E}D_{HEX2} + \dot{E}D_{OT} + \dot{E}D_{pump} + \dot{E}D_{intercooler} + \dot{E}D_{cond} \quad (18)$$

$$\dot{E}D_{conf\,2} = \dot{E}D_{HEX1} + \dot{E}D_{HT} + \dot{E}D_{LT} + \dot{E}D_{HTR} + \dot{E}D_{comp\,2} + \dot{E}D_{comp\,1} + \dot{E}D_{LTR} + \dot{E}D_{HEX2} + \dot{E}D_{OT\,1} + \dot{E}D_{OT\,2} + \dot{E}D_{intercooler} + \dot{E}D_{pump\,1} + \dot{E}D_{pump\,2} + \dot{E}D_{cond} \quad (19)$$

On the basis of the thermal modeling, numerous mathematical relations are used in the performance analysis of the solar power tower powered combined cycle have been discussed below;

Combined cycle exergy efficiency is determined as [31,33];

$$\eta_{ex\,standalone} = 1 - \frac{\dot{E}D_{standalone}}{\dot{E}_{solar}} \quad (20)$$

$$\eta_{ex\,conf\,1} = 1 - \frac{\dot{E}D_{conf\,1}}{\dot{E}_{solar}} \quad (21)$$

$$\eta_{ex\,conf\,2} = 1 - \frac{\dot{E}D_{conf\,2}}{\dot{E}_{solar}} \quad (22)$$

The combined cycle's thermal efficiency can also be defined by the relation between thermal and exergy efficiency of the combined cycle [31];

$$\eta_{th} = \eta_{ex} \cdot \eta_{Carnot} \quad (23)$$

Waste heat recovery ratio (WHRR) is a performance parameter is to be defined which represents the capacity to recover waste heat from the topping cycle. It is defined as the ratio of the net power output (net power output of ORC) to the maximum available waste heat to be recovered from waste heat source [34]. WHRR for the bottoming cycle is expressed as;

$$WHRR = \frac{\dot{W}_{net,ORC}}{\dot{m}_{sCO2} \cdot (h_{HEX2} - h_0)} \quad (24)$$

Where, h_0 and h_{HEX2} are the enthalpy of waste heat of the topping cycle at environmental temperature and at the inlet of HEX2 respectively. $\dot{m}_{sCO2}$ is mass flow rate of the sCO_2 flowing in topping cycle.

Modeling equations of the SPT powered combined cycle were solved in engineering equation solver (EES) [35].

Validation of the proposed cycles

In order to ensure the correct use of the modeling equation, previous studies were used to validate the current cycles. There is no availability of the literature on combined cascade sCO_2 cycle with intercooling and ORC/PDORC. Therefore, both toping and bottoming cycles

Table 4. Validation of different cycles

Validation of toping cascade sCO_2 cycle with intercooling				
Working fluid	**Baseline conditions**	**Thermal efficiency**		**Estimated error**
		Kim et al. [17]	**Current model**	
sCO_2	HT inlet pressure=27.46 MPa, HT inlet temperature = 494.17 °C, Compressor-1 inlet pressure = 6.57 MPa, Compressor-1 inlet temperature =36.8 °C, $\eta_{comp\,1}$ = 0.85, η_{HT} = 0.9	28.61%	28.59%	-0.06%
Validation of bottoming basic ORC				
Isopentane	OT inlet pressure= 3.023 MPa, OT inlet temperature = 184.1 °C, OT outlet pressure = 0.1515 MPa, η_{OT} = 0.6, η_{Pump} = 0.5,	Clemente et al. [36] 12%	Current model 12.1%	0.83%
R245fa	OT inlet pressure = 3.395 MPa, OT inlet temperature = 154.2 °C, OT outlet pressure= 0.2504 MPa, η_{OT} = 0.6, η_{Pump} = 0.5	11%	11.2%	0.18%
Validation of bottoming PDORC				
R245fa	Heat source temperature = 110 °C η_{OT} = 0.82, η_{Pump} = 0.72	Dai et al. [24] 6.37%	Current model 6.41%	-0.627%

were validated separately with existing literature as listed in table 4. Thermal efficiency has been taken as the validation parameter for both the cycles. Cascade sCO_2 with intercooling cycle was validated with the previous study Kim et al. [17]. Apart from this, bottoming ORC and PDORC were also validated with previous studies Clemente et al. [36] and Dai et al. [24] respectively at same baseline conditions respective to references. Thermal efficiency of the both topping and bottoming cycle was found nearly to the respective previous research as shown in table 4. However, present study was performed with input parameters that are different from the previous studies those were used for the validation purpose.

RESULTS AND DISCUSSION

Current study deals with the performance evaluation and comparison of the solar power tower driven cascade sCO_2 cycle with intercooling with basic ORC and parallel double evaporator ORC (PDORC). Simulation of the current systems has been performed with the help of EES. Effects of the variable on the system performance have been investigated keeping constant all other variable as listed in table 1.

System performance evaluation with solar irradiation

The system's thermal efficiency is also based on solar irradiation. Base condition of solar irradiation has been taken as 850 W/m^{2}as per Indian climate at Mumbai. As the current combined model is powered by a solar power tower, the effects of solar irradiation on the efficiency of the system must therefore be investigated. With solar irradiation, the exergy efficiency of the combined cycle has been continuously increased. The explanation behind this is that the solar concentrator field efficiently utilizes increased solar irradiation. This corresponds to an increase in the inlet exergy of the combined cycle [33]. According to the left axis of Figure 3, maximum exergy efficiency for standalone cycle, configuration-1, and configuration-2 was 69.76%, 70.86%, and 72.98% for the 950 W/m^2 of solar irradiation. At 950 W/m^2 of solar irradiation, the exergy efficiency of the intercooled cascade sCO_2 was enhanced by 1.57% and 4.61%, respectively, by integrating the basic ORC and the PDORC. It can be observed that improvement in the exergy efficiency with PDORC is more than the basic ORC. Because PDORC recovered more heat compared to the basic ORC due to the double evaporators. Additional heat was recovered from the intercooler by the incorporating the PDORC.

With solar irradiation, net power output and thermal efficiency of the system have also increased. At 950 W/m^2 of solar irradiation, configuration-2 achieved the highest thermal efficiency and net power output of 50.38% and 273.3 kW, respectively, as indicated in the right axis of Figures 3 and 4. The curve for thermal efficiency and power output has the same pattern as the curve for energy efficiency. The explanation behind this is that thermal efficiency is directly linked to exergy efficiency [31]. Increase in solar irradiation from 400 to 950 W/m^2, the thermal efficiency of the standalone cycle, configuration-1 and configuration-2 were increased from 26.76% to 47.23%, 27.89% to 48.3% and 30.06% to 50.38% respectively.

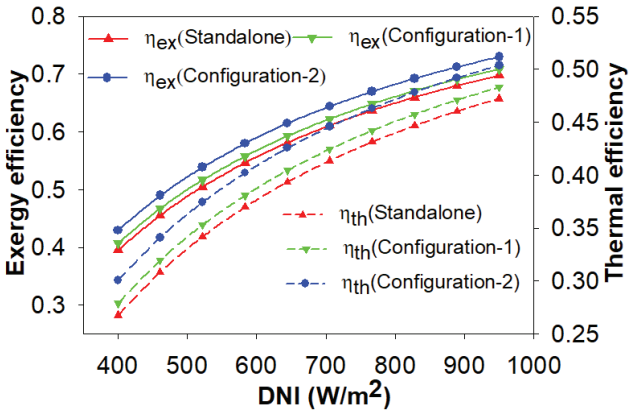

Figure 3. Exergy efficiency and thermal efficiency variation with the solar irradiation.

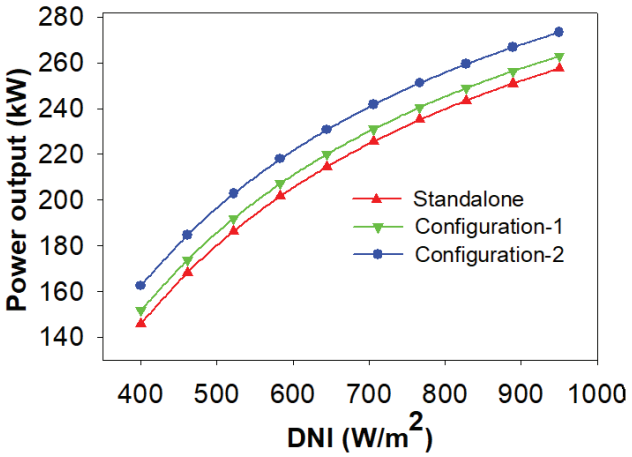

Figure 4. Power output variations with solar irradiation.

Performance evaluation with solar emittance

Solar emittance is the important parameter to be examined because it affects the receiver performance. It is seen in Figure 5, both exergy efficiency and thermal efficiency of the combined cycle decreases with the solar emittance. Receiver's surface temperature is the function of the solar emittance. Receiver efficiency decreases with the solar emittance. That means more heat loss to the surrounding, consequently less heat available to the combined cycle. As a result, the combined cycle's exergy efficiency and thermal efficiency are reduced. Increase in solar emittance from

0.05 to 0.2 reduces the exergy efficiency and thermal efficiency of configuration-2 by 3.57% and 6.28% respectively. As far as we know, all of the cycles operate under the identical input conditions, with the exception of bottoming cycles like ORC/PDORC. As a result, the curve pattern is consistent across all combinations. The similar effect of solar emittance was seen in the other two configurations as well.

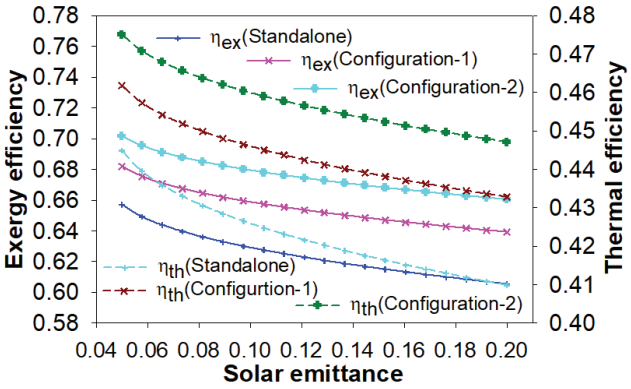

Figure 5. Exergy efficiency and thermal efficiency variation with solar emittance.

Performance evaluation with the concentration ratio

Another receiver design parameter to consider is the concentration ratio, which has an impact on the combined system's performance. As illustrated in Figure 6, increasing the concentration ratio increases combined cycle exergy efficiency and thermal efficiency. As the concentration ratio rises, the receiver efficiency rises, causing the HTF outlet temperature to rise, as the turbine inlet temperature is inversely proportional to the receiver outlet temperature. As a result, as the temperature of the turbine inlet grew, the combined cycle efficiency increased. The configuration-2 achieved the highest exergy efficiency and thermal efficiency once again. Exergy efficiency and thermal efficiency rise by 7.85% and 56.25%, respectively, when the concentration ratio is increased from 200 to 1400.

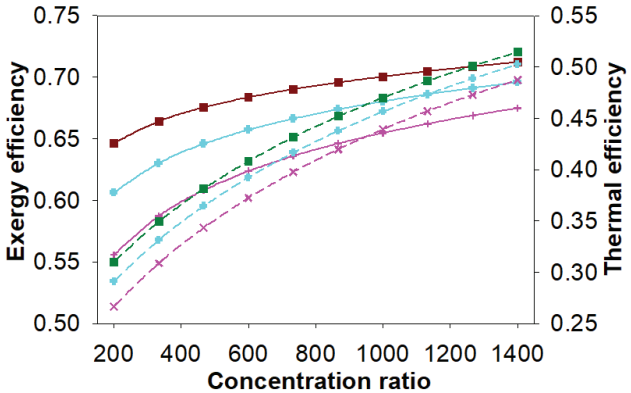

Figure 6. Exergy efficiency and thermal efficiency variation with the concentration ratio.

Performance evaluation with HT inlet temperature

The temperature of the molten salt has a direct impact on the HT inlet temperature (HTIT). HTIT rises in proportion to the molten salt's temperature. The heat loss in the solar receiver will, however, increase as the temperature of the molten salt rises. This results in lower receiver efficiency [8]. However, in the present study, the parameters of the solar field are kept constant and shown in Table 1. The main objective is therefore to compare the thermal performance of the standalone cycle with configuration-1 and configuration-2.

While investigating the effects of HTIT, other input parameters have been kept constant as shown in Table 1. The exergy efficiency, thermal efficiency and power output have increased with HTIT as can be seen in Figures 7 and 8 respectively. The reason behind increased efficiency and power output is that as HTIT increases the enthalpy difference across the HT, resulting in increased output power [15]. However, efficiency and output power have a different trend as HTIT increases, as shown in Figures 7 and 8.The highest thermal performance was achieved with configuration-2. At 800°C of

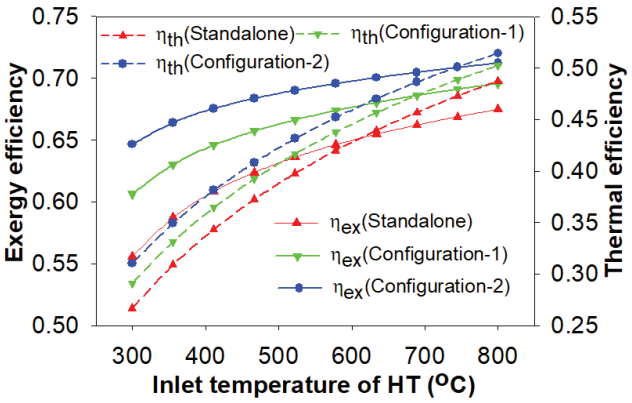

Figure 7. Exergy efficiency and thermal efficiency variation with inlet temperature of HT.

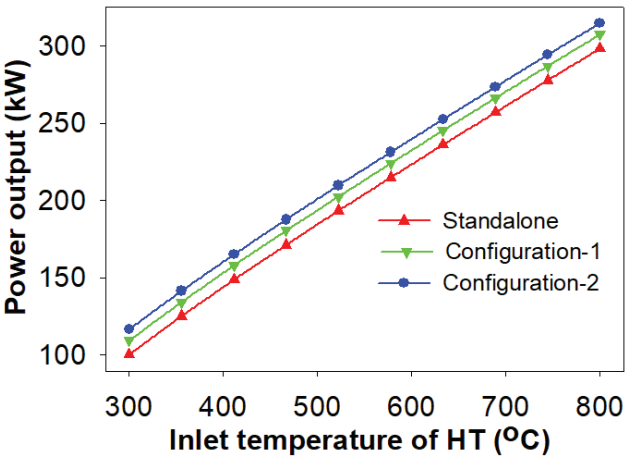

Figure 8. Power output variation with inlet temperature of HT.

HTIT, the highest exergy efficiency, thermal efficiency, and power production of configuration-2 were 71.22%, 51.43%, and 314.9 kW, respectively. Efficiency and output power are therefore highest with higher input thermodynamic variables. However, higher thermal performance cannot be achieved due to safety and material limitations. Although at same solar irradiation supercritical carbon dioxide cycle achieved higher efficiency than the superheated steam cycle at higher input turbine conditions [37,43].

Performance evaluation with the compressor-1 inlet pressure

It was observed that in the subcritical region where the pressure is below the critical value of 7.38 MPa the thermal and exergy efficiency increases with compressor-1 inlet pressure. Beyond the critical pressure of sCO_2, thermal and exergy efficiency increase and thereafter decrease. This indicates that there is a pressure point at which net power output and efficiency are at their maximum values. Exergy efficiency, thermal efficiency, and output power of the system have a bell-shaped curve as can be seen in Figures 9 and 10 respectively. The explanation for this pattern is that at critical pressure, the highest density of CO_2 results in decreased compression power [38]. As a result, the highest net power output and thus the best thermal and exergy efficiency are achieved. In the case of configuration-2, the best thermal performance was achieved. As shown in Figures 9 and 10, the configuration-2 achieved the highest exergy efficiency, thermal efficiency, and output power of 73%, 49.42%, and 269.4 kW at an optimum pressure of 7.74 MPa.

Performance evaluation with compressors inlet temperature

The intercooling has been assumed to be perfect in this investigation. That is, following the compressor-1, the intercooler lowers the sCO_2 stream temperature to the compressor-1's inlet temperature. The compressor's inlet temperature has an impact on system performance. The influence of the CsIT on system performance was investigated while the other input parameters were kept constant as shown in Table 1. The compressor-1 inlet pressure has been fixed at 7.5 MPa. The CsIT ranges from 32°C to 38°C. The thermal performances of the all configurations were decreased with the CsIT as shown in Figures 11 and 12. The

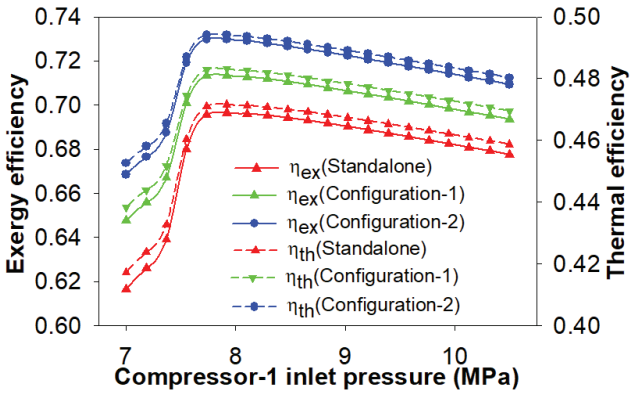

Figure 9. Exergy efficiency and thermal efficiency variation with compressor-1 inlet pressure.

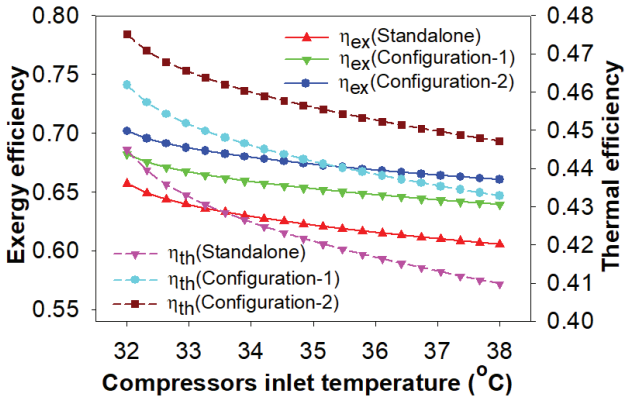

Figure 11. Exergy efficiency and thermal efficiency variation with compressors inlet temperature.

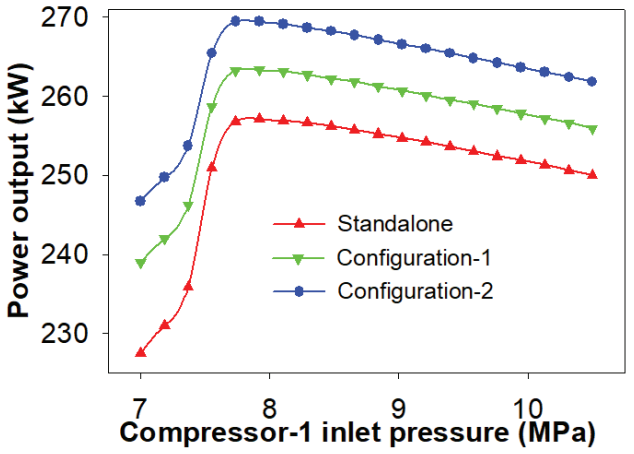

Figure 10. Power output variation with compressor-1 inlet pressure.

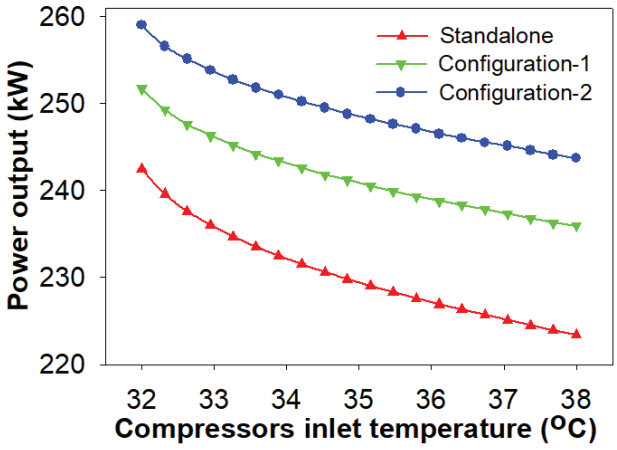

Figure 12. Power output variation with compressors inlet temperature.

reduction in thermal performance of the system is due to the fact that as the temperature rises over the critical state of CO_2, the CO_2's specific heat falls, resulting in a decreased enthalpy at the compressor-1 inlet [39]. This results in a greater enthalpy differential across the compressor, resulting in increased input power. As a result, the net power output is reduced. The heat available at the inlet to the combined cycle is known to be constant, depending on the SPT parameters [15]. As a result, the efficiency and net output of the combined cycle were reduced with the CsIT. It was also shown that the total decrease in thermal performance of the combined system was due to the standalone sCO_2 cascade cycle. As seen due to increse in CsIT performance of bottoming ORC also sligtly decreased due to slight decrement in turbine output. Therefore, the performance of the bottoming ORC was not significantly affected by the variation of the CsIT. It is shown that configuration-2 perfomed well among other configurations. As a result, the configuration-2's highest exergy efficiency, thermal efficiency, and power output were 70.17%, 47.51%, and 259 kW at 32°C of CsIT, respectively, as shown in Figures 11 and 12.

Effects on waste heat recovery ratio

Main objective of the current study is to compare the effect of basic ORC (configuration-1) and PDORC (configuration-2) to recover the waste heat. That means which system is better to recover the waste heat configuration-1 or configuration-2. WHRR is for the configuration-2 is more than the configuration-1. That means PDORC recovered more heat than basic ORC. At 0.95 effectiveness of HEX2, the highest WHRR for configuration-1 and configuration-2 was 0.1372 and 0.2016, respectively. As a result, the PDORC recovers 46.93% more heat than the ORC, as shown in Figure 13. With the effectiveness of HEX2, WHRR increased continuously. As the recovery of waste heat in HEX2 is increased with effectiveness, the increase in WHRR with HEX2 effectiveness can be clarified. As a result, more enthalpy leads to improved work output across the ORC turbine [15]. As a result, according to the Eq. (24), WHRR increased.

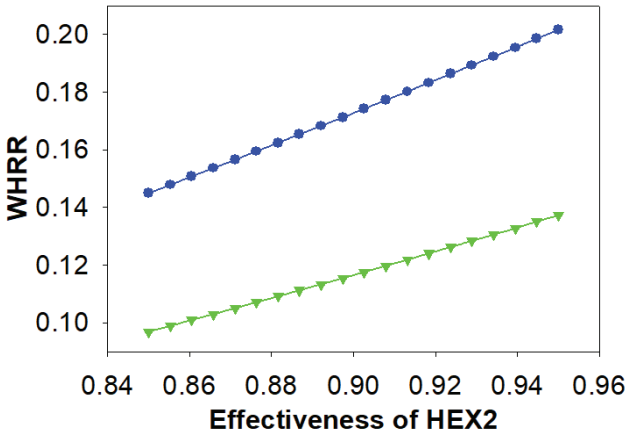

Figure 13. WHRR variation with effectiveness of HX2.

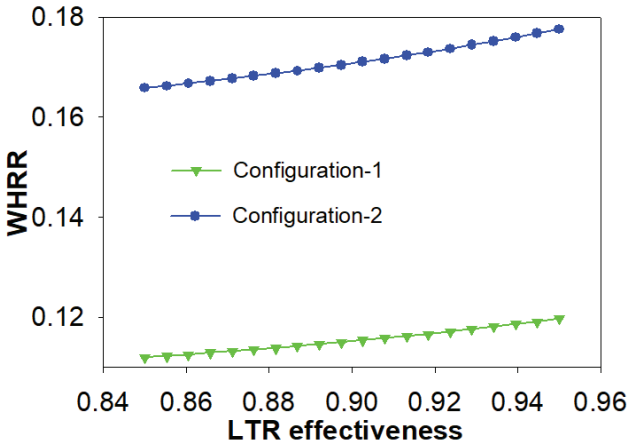

Figure 14. WHRR variation with LTR effectiveness.

Table.5. Optimum major results calculated at 950 W/m^2 of DNI

Parameters	Values
Best configuration	Configuration-2
Highest thermal efficiency	50.38%
Highest exergy efficiency	72.98%
Highest power output	273.3kW
Highest improvement in thermal efficiency	4.61%
Highest improvement in exergy efficiency	6.66%
Maximum WHRR	0.1775

Effect of the effectiveness of the LTR on the performance of the ORC was also examined further in this section. WHRR was slightly increased with the effectiveness of the LTR as shown in Figure 14. The reason behind this is that when the effectiveness of the LTR is increased, more heat is recovered by the cold stream of the sCO_2. This leads to a lower sCO_2 temperature at inlet to HEX2. In other words, the low heat at the inlet to the HEX2 can be said. It reduces the inlet temperature of the ORC turbine. As a result, the lower inlet temperature of the ORC turbine increases the output power of the ORC turbine in case of organic working fluids [40]. On the other hand at inlet of HEX2 enthalpy also decreases because of lower heat at the HEX2 inlet. As a result, WHRR increased with the LTR effectiveness according to the Eq. (24). WHRR for the configuration-2 is more than the configuration-1. At 0.95 LTR effectiveness, the maximum WHRR for configuration-1 and configuration-2 was 0.1197 and 0.1775, respectively, as shown in Figure 14. Apart from all these, calculated major results from result ant discussion section are listed in the table 5 for better understanding.

CONCLUSIONS

From the result and discussions sections following conclusions were made.

- Thermal performance of system increased with solar irradiation. The standalone cycle, configuration-1 and configuration-2 show maximum exergy efficiency of 69.76%, 70.86% and 72.98% respectively at the 950 W/m^2 of solar irradiation.
- By incorporating the basic ORC and the PDORC to the intercooled cascade sCO_2 cycle, exergy efficiency were improved by 1.57% and 4.61% while thermal efficiency improved by 2.26% and 6.66% respectively at 950 W/m^2 of solar irradiation.
- System performance falls as solar emittance increases, but increases when the concentration ratio increases. As a result, in order to improve the combined cycle's performance, the solar emittance must be reduced and the concentration ratio must be increased.
- The highest exergy efficiency, thermal efficiency and output power of the configuration-2 were achieved as 73%, 49.42% and 269.4 kW at an optimum pressure of 7.74 MPa of compressor-1 inlet pressure.
- At 0.95 of LTR effectiveness, the maximum WHRR for configuration-1 and configuration-2 was 0.1197 and 0.1775, respectively.
- The PDORC recovered 48.28% more waste heat than the basic ORC. Therefore, configuration-2 is more suitable to recover the waste heat completely.
- Finally, it was highly recommended to design the SPT system carefully to get better performance of the combined cycle.

NOMENCLATURE

A_h	Heliostat area (m^2)
DNI	Direct normal irradiation (W/m^2)
$\dot{Q}_h$	Actual solar heat received by heliostat field (kW)
$\dot{E}_{solar}$	Solar exergy (kW)
$\dot{E}$	Exergy rate (kW)
f_{view}	Receiver's view factor
h_{conv}	Coefficient for convection heat loss (W/ m^2-K)
s	specific entropy (kJ/kg-K)
N_h	Number of heliostat
$\dot{m}$	Mass flow rate (kg/s)
$\dot{Q}_{solar}$	Solar heat received by heliostat field (kW)
$\dot{W}$	Power (kW)
h	specific enthalpy (kJ/kg)
T	Temperature (K)
Cp	Specific heat (kJ/kg-K)
sCO_2	Supercritical carbon dioxide
$\dot{E}D$	Rate of exergy destruction (kW)
T_R	Receiver surface temperature (K)
$\dot{Q}$	Heat rate in (kW)
SPT	solar power tower
η_h	Heliostat efficiency
η_{th}	Thermal efficiency
x	Fraction of mass of sCO_2
η_{ex}	Exergy efficiency
η_r	Receiver thermal efficiency
$\dot{Q}_{loss,r}$	Heat loss from the receiver (kW)
$\dot{Q}_r$	Heat received by central receiver (kW)

Abbreviations

Comp 1	Compressor-1
Comp 2	Compressor-2
Cond	condenser
Conf 1	configuration-1
Conf 2	configuration-2
CR	concentration ratio
CsIT	Compressors inlet temperature (°C)
CV	Control volume
HEX1	heat exchanger-1
HEX2	heat exchanger-2
HT	High temperature turbine
HTIT	High turbine inlet temperature (°C)
HTR	High temperature recuperator
LT	Low temperature turbine
LTR	Low temperature recuperator
ORC	Organic Rankine cycle
OT	ORC turbine
OT1	ORC turbine-1
OT2	ORC turbine-2
PDORC	Parallel double evaporator ORC
WHRR	Waste heat recovery ratio

Subscripts

e	exit
0	dead condition
r	receiver
h	heliostat
i	inlet
j	particular atate
su	Sun
ms	molten salt

Greek letters

η	Efficiency
ε	Effectiveness
α	Solar absorbance
δ	Change in property
β	Sun's subtended cone half angle(rad)
σ	Stephen Boltzmann constant (W/m)

AUTHORSHIP CONTRIBUTIONS

Authors equally contributed to this work.

DATA AVAILABILITY STATEMENT

The authors confirm that the data that supports the findings of this study are available within the article. Raw data that support the finding of this study are available from the corresponding author, upon reasonable request.

CONFLICT OF INTEREST

The author declared no potential conflicts of interest with respect to the research, authorship, and/or publication of this article.

ETHICS

There are no ethical issues with the publication of this manuscript.

REFERENCES

[1] Mustafa AA, Noranai Z, Imran AA. Solar absorption cooling systems: A review. J Therm Eng 2021;7:970−983. [CrossRef]

[2] Ghasemi A, Shayesteh AA, Doustgani A, Pazoki M. Thermodynamic assessment and optimization of a novel trigeneration energy system based on solar energy and MSW gasification using energy and exergy concept. J Therm Eng 2021;7:349−366. [CrossRef]

[3] Kabira E, Kumar P, Kumar S, Adelodund AA, Kime K. Solar energy: Potential and future prospects. Renew Sustain Energy Rev 2018;82:894−900. [CrossRef]

[4] Toujeni N, Bouaziz N, Kairaouani L. Energetic investigation of a new combined ORC−VCC system for cogeneration. Energy Procedia 2017;139:670−675. [CrossRef]

[5] Kalogirou SA. Solar thermal collectors and applications. Prog Energy Combust Sci 2004;30:231−295. [CrossRef]

[6] Fuqiang W, Ziming C, Jianyu T, Yuan Y, Yong S, Linhu L. Progress in concentrated solar power technology with parabolic trough collector system: A comprehensive review. Renew Sustain Energy Rev 2017;79:1314−1328. [CrossRef]

[7] Farges O, Bézian J, El-Hafi M. Global optimization of solar power tower systems using a Monte Carlo algorithm: Application to a redesign of the PS10 solar thermal power plant. Renew Energy 2018;119:345−353. [CrossRef]

[8] Khatoon S, Kim M. Performance analysis of carbon dioxide based combined power cycle for concentrating solar power. Energy Convers Manag 2020;20:112416. [CrossRef]

[9] Alsagri AS, Chiasson A, Gadalla M. Viability assessment of a concentrated solar power tower with a supercritical CO_2 brayton cycle power plant. J Sol Energy Eng 2018;145:051006. [CrossRef]

[10] Ma Y, Morozyuk T, Liu M, Yan J, Liu J. Optimal integration of recompression supercritical CO_2 Brayton cycle with main compression intercooling in solar power tower system based on exergoeconomic approach. Appl Energy 2019;242:1134−1154. [CrossRef]

[11] Shukla AK, Sharma A, Sharma M, Nandan G. Thermodynamic investigation of solar energy-based triple combined power cycle. Energy Sources A: Recovery Util Environ Eff 2019;41:1161−1179. [CrossRef]

[12] Abid M, Adebayo VO, Atikol U. Energetic and exegetic analysis of a novel multi-generation system using solar power tower. Int J Exergy 2019;29:211. [CrossRef]

[13] Ahn Y, Bae SJ, Kim M, Cho SK, Baik S, Lee JI, et al. Review of supercritical CO_2 power cycle technology and current status of research and development, Nucl Eng Technol 2015;47:647−661. [CrossRef]

[14] Khan Y, Mishra RS. Parametric (exergy-energy) analysis of parabolic trough solar collector-driven combined partial heating supercritical CO_2 cycle and organic Rankine cycle. Energy Sources A Recovery Util Environ Eff 2020;1−27. [CrossRef]

[15] Khan Y, Mishra RS. Performance evaluation of solar-based combined pre-compression supercritical CO_2 cycle and organic Rankine cycle. Int J Green Energy 2020;18:172−186. [CrossRef]

[16] Besarati SM, Goswami DY. Analysis of advanced supercritical carbon dioxide power cycles with a bottoming cycle for concentrating solar power applications. J Sol Energy Eng 2014;136:010904. [CrossRef]

[17] Kim MS, Ahn Y, Kim B, Lee JI. Study on the supercritical CO_2 power cycles for landfill gas firing gas turbine bottoming cycle. Energy 2016;111:893−909. [CrossRef]

[18] Yu W, Gong Q, Gao D, Wang G, Su H, and Li X. Thermodynamic analysis of supercritical carbon dioxide cycle for internal combustion engine waste heat recovery. Processes 2020;8:216. [CrossRef]

[19] Neises T, Turchi C. Supercritical carbon dioxide power cycle design and configuration optimization to minimize levelized cost of energy of molten salt power towers operating at 650 °C. Sol Energy 2019;181:27−36. [CrossRef]

[20] Kimzey G. Development of a Brayton bottoming cycle using supercritical carbon dioxide as the working fluid, a report submitted in partial fulfillment of the requirements for gas turbine industrial fellowship. University Turbine Systems Research Program, University Turbine Systems Research Program, 2012.

[21] Shaaban S. Analysis of an integrated solar combined cycle with steam and organic Rankine cycles as bottoming cycles. Energy Convers Manag 2016;126:1003−1012. [CrossRef]

[23] Song J, Li X, Ren X, Gu C. Performance analysis and parametric optimization of supercritical carbon dioxide (S-CO_2) cycle with bottoming Organic Rankine Cycle (ORC). Energy 2018;143:406−416. [CrossRef]
[24] Dai Y, Hu D, Wu Y, Gao Y, Cao Y. Comparison of a basic organic rankine cycle and a parallel double-evaporator organic rankine cycle. Heat Transf Eng 2017;38:990−999. [CrossRef]
[25] Bejan A, Kearney DW, Kreith F. Second law analysis and synthesis of solar collector systems. J Sol Energy Eng Trans 1981;103:23−28. [CrossRef]
[26] Ho CK, Iverson BD. Review of high-temperature central receiver designs for concentrating solar power. Renew Sustain Energy Rev 2014;29:835−846. [CrossRef]
[27] Wang X, Liu Q, Lei J, Han W, Jin H. Investigation of thermodynamic performances for two-stage recompression supercritical CO_2 Brayton cycle with high temperature thermal energy storage system. Energy Convers Manag 2018;165:477−487. [CrossRef]
[28] Neises T, Turchi C. A Comparison of Supercritical Carbon Dioxide Power Cycle Configurations with an Emphasis on CSP Applications. Energy Procedia 2014;49:1187−1196. [CrossRef]
[29] Reyes-Belmonte MA, Sebastián A, Romero M. Optimization of a recompression supercritical carbon dioxide cycle for an innovative central receiver solar power plant. Energy 2016;112:17−27. [CrossRef]
[30] Xu X, Wang X, Li P, Li Y, Hao Q, Xiao B, et al. Experimental test of properties of KCl-MgCl2 eutectic molten salt for heat transfer and thermal storage fluid in concentrated solar power systems. J Sol Energy Eng 2018;140:051011. [CrossRef]
[31] Cengel YA, Boles MA. Thermodynamics An Engineering Approach. 5th ed. New York:McGraw−Hill; 2004.
[32] Parrott JE. Theoretical upper limit to the conversion efficiency of solar energy. Sol Energy 1978;21:227−229. [CrossRef]
[33] Al-Sulaiman FA. Exergy analysis of parabolic trough solar collectors integrated with combined steam and organic Rankine cycles. Energy Convers Manag 2014;77:441−449. [CrossRef]
[34] Kim YM, Shin DG, Kim CG, Cho GB. Single-loop organic Rankine cycles for engine waste heat recovery using both low- and high-temperature heat sources. Energy 2016;96:482−494. [CrossRef]
[35] Klein SA. Engineering Equation Solver (EES), Academic Commercial V7.714. F-Chart Software 2020. Accessed on May 03, 2023. Available at: www.fChart.com.
[36] Clemente S, Micheli D, Reini M, Taccani R. Bottoming organic Rankine cycle for a small scale gas turbine: a comparison of different solutions. Appl Energy 2013;106:355−364. [CrossRef]
[37] Chacartegui R, Muñoz JM, Escalona D, Sánchez D, Monje B, Sánchez T. Alternative cycles based on carbon dioxide for central receiver solar power plants. Appl Therm Eng 2011;31:872−879. [CrossRef]
[38] Blanco MJ, Santigosa LR. Advances in concentrating solar thermal research and technology. 1st ed. United Kingdom: Elsevier; 2017.
[39] Chen Y, Lundqvist P. The CO_2 transcritical power cycle for low grade heat recovery discussion on temperature profiles in system heat exchangers. Proceedings of the ASME Power Conference POWER; 2011 July 12-14; Denver, Colorado, USA: ASME; 2011. pp. 385−392. [CrossRef]
[40] Dai Y, Wang J, Gao L. Parametric optimization and comparative study of organic Rankine cycle (ORC) for low grade waste heat recovery. Energy Convers Manag 2009;50:576−582. [CrossRef]
[41] Khan Y, Mishra RS. Thermo-economic analysis of the combined solar based pre-compression supercritical CO_2 cycle and organic Rankine cycle using ultra low GWP fluids. Therm Sci Eng Prog 2021;23:100925. [CrossRef]
[42] Khan Y, Mishra RS. Performance analysis of solar driven combined recompression main compressor intercooling supercritical CO_2 cycle and organic Rankine cycle using low GWP fluids. Energy Built Environ 2021;3:496−507. [CrossRef]
[43] Khan Y, Mishra RS. Performance comparison of the solar-driven supercritical organic Rankine cycle coupled with the vapour-compression refrigeration cycle. Clean Energy 2021;5:476−491. [CrossRef]